Molecular Therapy
Nucleic Acids
Original Article

Targeted SHP-1 Silencing Modulates the Macrophage Phenotype, Leading to Metabolic Improvement in Dietary Obese Mice

Yadhu Sharma,[1] Altaf Ahmad,[2] Prabhu Srinivas Yavvari,[3] Sandeep Kumar Muwal,[4] Avinash Bajaj,[4] and Farah Khan[1]

[1]Department of Biochemistry, School of Chemical & Life Sciences, Jamia Hamdard, New Delhi 110062, India; [2]Department of Botany, Aligarh Muslim University, Aligarh, Uttar Pradesh 202001, India; [3]Institute for Chemistry & Biochemistry, Freie University, Berlin 14195, Germany; [4]Laboratory of Nanotechnology and Chemical Biology, Regional Centre of Biotechnology, Faridabad, Haryana 121001, India

Chronic over-nutrition promotes adipocyte hypertrophy that creates inflammatory milieu leading to macrophage infiltration and their phenotypic switching during obesity. The SH2 domain-containing protein tyrosine phosphatase 1 (SHP-1) has been identified as an important player in inflammatory diseases involving macrophages. However, the role of SHP-1 in modulating the macrophage phenotype has not been elucidated yet. In the present work, we show that adipose tissue macrophage (ATM)-specific deletion of SHP-1 using glucan particle-loaded siRNA improves the metabolic phenotype in dietary obese insulin-resistant mice. The molecular mechanism involves AT remodeling via reducing crown-like structure formation and balancing the pro-inflammatory (M1) and anti-inflammatory macrophage (M2) population. Therefore, targeting ATM-specific SHP-1 using glucan-particle-loaded SHP-1 antagonists could be of immense therapeutic use for the treatment of obesity-associated insulin resistance.

INTRODUCTION

Chronic overnutrition and obesity lead to "meta-inflammation," a state of low-grade inflammation throughout the body that has been etiologically linked to the pathogenesis of obesity-induced insulin resistance and metabolic syndrome. Liver, skeletal muscle, and adipose tissue are three major insulin-targeted tissues involved in glucose utilization. The initiation of inflammation in adipose tissue is considered the driving factor for meta-inflammation leading to systemic insulin resistance.[1] Immune cell fraction of adipose tissue, i.e., stromal vascular fraction (SVF) and specifically the adipose tissue macrophages (ATMs), plays an important part in this process.[2] AT responds to nutrient excess via adipocyte hypertrophy and hyperplasia. The expanding AT secretes various chemotactic factors that recruit immune cells into the AT. Monocyte chemoattractant protein-1 (MCP-1) causes recruitment of blood monocytes as ATMs that orchestrate AT inflammation by cytokine-mediated polarization.[3,4] Obesity-associated inflammation leads to accumulation of CD11c-expressing ATMs.[4] These cells display an inflammatory M1-like phenotype, releasing inflammatory cytokines such as tumor necrosis factor α (TNF-α), interleukin-1β (IL-1β), and IL-6, that promote insulin resistance.[5] In contrast, lean AT in insulin-sensitive mice is mainly populated with $CD11c^{-}$ anti-inflammatory M2-like phenotype macrophages that secrete anti-inflammatory cytokines (IL-10 and IL-4).[6] Therefore, reshaping the immunological status of AT via modulating the macrophage phenotype is a promising strategy to achieve therapeutic advancement in obesity-induced insulin resistance. For example, ATM-specific silencing of TNF-α, matrix metalloproteinase-12 (MMP12), and C-C chemokine receptor type 2 (CCR2) has been shown to improve insulin sensitivity via suppressing AT inflammation.[7–9]

SH2 domain-containing protein tyrosine phosphatase 1 (SHP-1) is a class I classical nonreceptor protein tyrosine phosphatase that has been proposed to contribute to glucose homeostasis. Improved glucose utilization and insulin sensitivity in viable motheaten ($Ptpn6^{me\text{-}v/me\text{-}v}$) mice expressing low levels of functionally deficit SHP-1 protein introduced the metabolic regulatory function of SHP-1.[10] Interestingly, adenoviral-mediated or small hairpin RNA-mediated SHP-1 silencing in liver augments hepatic insulin signaling and glucose utilization.[10,11]

Apart from genetic deletion, the pharmacological inhibition of SHP-1 using sodium stibogluconate, a known inhibitor of SHP-1, was efficient in ameliorating the metabolic phenotype in a mouse model of high-fat-diet (HFD)-induced insulin resistance.[12] Additionally, the anti-hyperglycemic and anti-inflammatory actions of metformin in an obese insulin-resistant mouse model were found to be associated with reduced SHP-1 expression and activity in AT.[13] To date, the studies involving the role of SHP-1 in glucose homeostasis has been limited to the metabolic aspect of the disease and does not investigate the inflammatory side of obesity-associated insulin resistance. Considering the implication of SHP-1 in the pathogenesis of macrophage-related inflammatory disorders including multiple sclerosis,[14] it is likely that the AT inflammation during obesity may involve

Received 15 December 2018; accepted 26 April 2019;
https://doi.org/10.1016/j.omtn.2019.04.020.

Correspondence: Farah Khan, Department of Biochemistry, School of Chemical & Life Sciences, Jamia Hamdard, New Delhi 110062, India.
E-mail: fkhan@jamiahamdard.ac.in

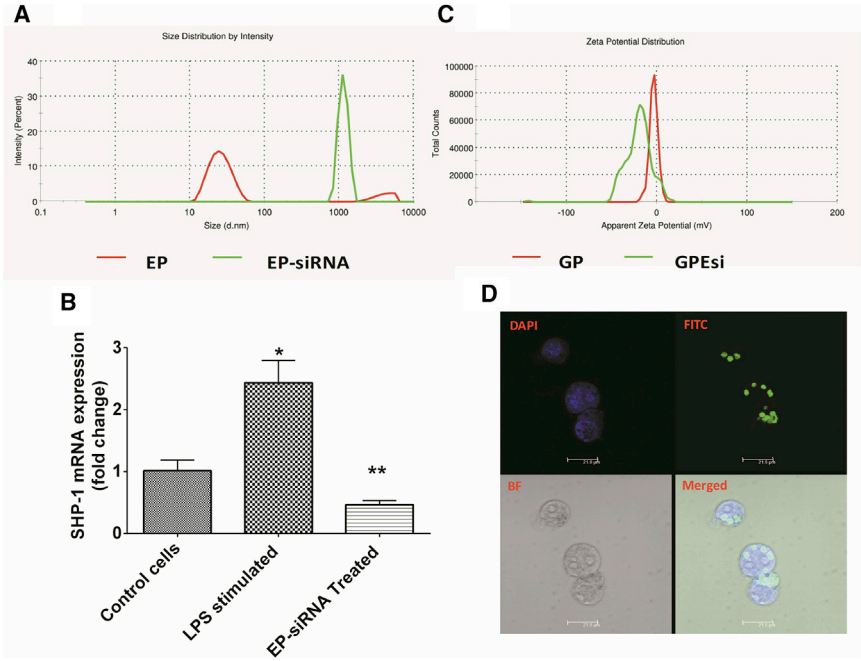

Figure 1. Preparation of EP-siRNA-Loaded Glucan Particles and SHP-1 Silencing in Murine Macrophages

(A) EP alone (red) or siRNA-EP (green) complex size was determined by DLS at 25°C. The result shows average particle size distribution from three independent measurements. (B) RAW264.7 cells were treated with LPS (100 ng/mL) or LPS + EP-siRNA and the fold change in SHP-1 mRNA levels are presented as means ± SEM, n = 3. Statistical significance was determined by ANOVA Tukey post-test. *$p < 0.05$, **$p < 0.01$ when LPS stimulated group was compared with RAW264.7 cells and EP-siRNA-treated group. (C) The zeta potential of glucan particles (GPs) and GPs with entrapped siRNA-EP complexes (GPEsi) shown in red and green, respectively. The result shows average zeta potential from three independent measurements. (D) Confocal microscopy images showing uptake of FITC-tagged GPs by RAW264.7 cells. Cells were counterstained by DAPI. Scale bar, 21.8 μm; BF, bright field.

modulation of the ATM phenotype by SHP-1. Recently, Zheng et al.[15] reported that CD11b regulates the proliferation and alternative activation of ATMs via regulating IL-4/signal transducer and activator of transcription 6 (STAT-6) axis, through the activity of SHP-1. Targeting ATM-specific SHP-1 could be a valuable approach to delineate the implication of SHP-1 in obesity-associated inflammation and may prove to be a potential remedy for the treatment of metabolic disturbances related to the same.

The hollow and porous glucan particles (GPs) derived from Baker's yeast allows absorption and retention of payload molecules (e.g., DNA, small interfering RNA [siRNA], and proteins) and their effective delivery via cell surface receptors in macrophages (dectin-1 [D1]).[16] The clinical potential of GPs encapsulated siRNA and their specific delivery into AT-resident macrophages upon intraperitoneal (i.p.) injection has already been studied.[7] Here, we report that the GP entrapped siRNA mediated SHP-1 silencing in ATMs tune up the M1 and M2 macrophage population and a subset of macrophage phenotype markers in AT, leading to metabolic improvement in the obese insulin-resistant model. Thus, glucan-particle-based targeted silencing of SHP-1 led to recognition of an unrevealed function of AT-specific SHP-1 in modulating AT physiology and the macrophage phenotype and the molecular mechanism behind the improved metabolic character in SHP-1-deficient mice.

RESULTS

Characterization of EP-siRNA Complex and SHP-1 Silencing in Murine Macrophages

The cell-type selectivity of GPs was utilized to specifically silence SHP-1 in murine macrophages. The Endo-Porter (EP)-siRNA complex was prepared, and the mean particle size was found to be 1,178 ± 20.80 nm with a polydispersity index of 0.56 ± 0.02, whereas EP alone showed mean particle size of 26.41 ± 0.02 nm with a polydispersity index of 0.40 ± 0.07 at pH 7.4 (Figure 1A). EP-siRNA-mediated SHP-1 silencing was confirmed by incubating the murine macrophage-like cell line, RAW264.7 with lipopolysaccharide (LPS) and EP-siRNA complex. Treatment of RAW264.7 cells with 150 pmol siRNA targeting SHP-1 induced an ~0.5-fold and ~2-fold reductions in target mRNA levels in comparison to control and LPS-stimulated cells, respectively (Figure 1B). Further, the loading of GPs with EP-siRNA complex (GPEsi) shifted the zeta potential from −4.76 ± 0.54 mV to −22.5 ± 0.8 mV, indicating the successful association of siRNA with the particles (Figure 1C). To assess the internalization of GPs, RAW264.7 cells were incubated with fluorescein isothiocyanate (FITC)-tagged GPs, counterstained with DAPI, and analyzed by confocal microscopy. Figure 1D shows the uptake of GPs by the cells.

Localization of GPs in High-Fat-Diet-Fed Mice

To analyze the localization of GPs, C57BL/6J mice were fed with high-fat diet (HFD-IR) for a period of 16 weeks and intraperitoneally injected with Cy7-tagged GPs. The *in vivo* imaging of the localized GPs was performed using an IVIS imaging system at excitation wavelength 753 nm and emission wavelength 800 nm (PerkinElmer) (Figure 2A). Just after the injection, there was an intense Cy7 signal from the peritoneal region, which diminished drastically after an hour due to fatty skin barrier (Figure S1). After 4 hr of intraperitoneal injection, the total radiance energy obtained from the epididymal AT region of HFD-IR mice injected with Cy7-labeled GPs (7.48E+08 ± 3.38E+06 (p/s)/(μW/cm^2)) was significantly higher ($p < 0.05$) than epididymal AT region of un-injected HFD-IR mice

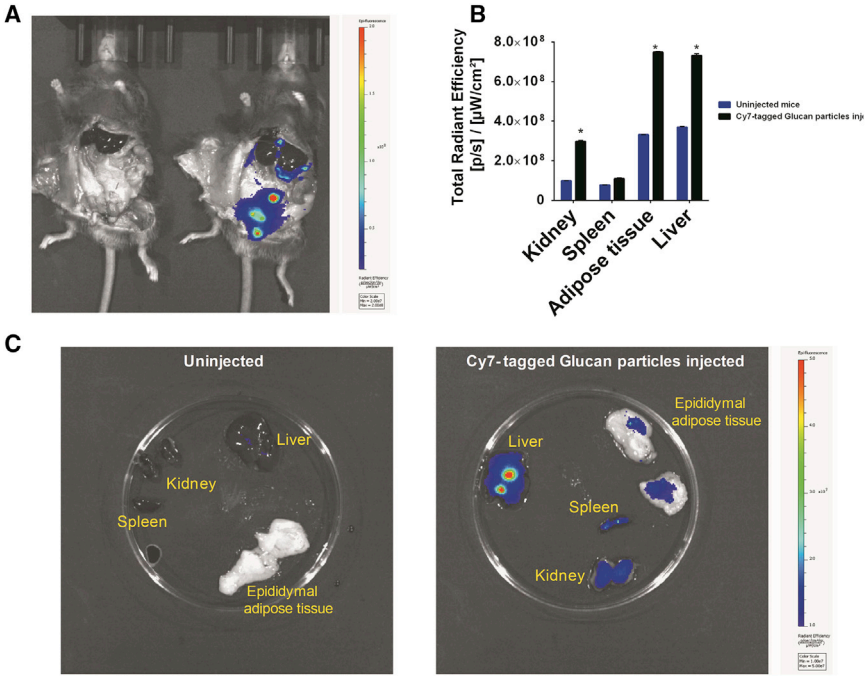

Figure 2. Localization of GPs in High-Fat-Diet-Fed Mice

(A) Whole-body IVIS images of high-fat-diet-fed mice uninjected (left) and injected (right) with Cy7-labeled GPs. (B) Graph showing total radiant efficiency ([p/s]/[μW/cm^2]) of IVIS imaged organs (liver, spleen, kidney, and epididymal adipose tissue). (C) Representative images of dissected organs (liver, spleen, kidney, and epididymal adipose tissue) from uninjected and Cy7-tagged GPs injected obese mice. Data are means ± SEM, n = 3. Unpaired t test, *p < 0.05 compared to uninjected high-fat-diet-fed mice.

(3.31e+008 ± 2.98E+05 (p/s)/(μW/cm^2)) suggesting rapid localization of GPs in epididymal AT (Figures 2B and 2C).

ATMs from HFD-IR Mice Uptake GPs

To confirm the internalization of FITC-tagged GPs by adipose-tissue (AT)-resident macrophages, the epididymal AT sections were stained with anti-F4/80, a marker for macrophages and analyzed by microscopy (Figure 3A). The FITC-tagged GPs were observed to be localized in the F4/80$^+$ cells that form a crown-like structure around the adipocyte. The results obtained show that epididymal AT resident macrophages internalize the i.p. injected GPs in HFD-IR mice.

ATM Specific Deletion of SHP-1 in HFD-IR Mice

C57BL/6J mice were fed with HFD for a period of 16 weeks and i.p. injected with GPs loaded with nontargeting or SHP-1 siRNA on alternate days for 2 weeks. Immunohistochemical analysis of AT stained with SHP-1 antibody showed a significantly marked staining (50%–75%) in the HFD-IR and non-targeting (NT) siRNA group in comparison to the lean group that showed less than 25% staining area (Figure 3B). The staining area showed SHP-1 expression within crown-like structures around adipocytes, suggesting SHP-1 is predominantly expressed by AT-resident immune cells (majorly macrophages). SHP-1 expression was significantly reduced in the SHP-1 siRNA group as observed by a marked decrease in staining area (<25%) (Figure 3B). Further, the genetic deletion of ATM-specific SHP-1 was confirmed by checking the SHP-1 mRNA using qPCR. There was a significant ~6-fold change in SHP-1 mRNA levels in HFD-IR-derived macrophages when compared to lean mice (Figure 3C). However, GPs loaded with SHP-1 siRNA efficiently downregulated SHP-1 expression as observed in the SHP-1 siRNA group. We observed a significant ~9-fold decrease in SHP-1 mRNA levels in the SHP-1 siRNA group in comparison to the HFD-IR group, whereas the NT siRNA group showed an increase in SHP-1 mRNA expression in comparison to HFD-IR group (Figure 3C). The data obtained showed that ATMs derived from the HFD-IR group display a significant increase in the expression of SHP-1 in comparison to ATMs isolated from lean mice and SHP-1 siRNA-loaded GPs, effectively downregulating SHP-1 expression in high-fat-diet-fed group. This is consistent with the earlier studies that demonstrated adipose-tissue-specific localization of GPs (glucan-encapsulated siRNA particles) and other carrier molecules upon intraperitoneal injection.[7,17,18]

ATM Specific Deletion of SHP-1 Leads to Improved Insulin Sensitivity in HFD-IR Mice

As consistent with previous findings, in comparison to the lean group, high-fat-diet-fed mice display metabolic dysfunction as characterized by significantly increased body weight, basal blood glucose, basal blood insulin, serum triglyceride, serum cholesterol, and epididymal fat pad weight (Figure 4). The high-fat-diet group had significantly increased ($p < 0.001$) body weight (42.8 ± 0.87 g) in comparison to the lean group (27.4 ± 1.32 g), which was a slightly reduced in SHP-1 siRNA group (40.50 ± 1.12 g) (Figure 4A). Also, the epididymal fat pads from the SHP-1 siRNA group also showed a nonsignificant reduction (2.84 ± 0.16 g) in weight in comparison to HFD-IR group (3.1 ± 0.10 g) (Figure 4B). Similarly, the HFD-IR group injected with NT siRNA did not show a significant change in body weight or epididymal fat pad weight from the HFD-IR or SHP-1 siRNA group (Figures 4A and 4B). The results suggest that SHP-1 downregulation have little impact on body weight.

To assess glucose utilization, an oral glucose tolerance test (OGTT) was performed that showed efficient glucose clearance from the bloodstream in the SHP-1 siRNA group in comparison to the HFD-IR group. In the SHP-1 siRNA group, the blood glucose levels were observed to significantly lower when compared to the HFD-IR group at 0 (168.4 ± 8.07 versus 126.4 ± 6.5 mg/dL), 15

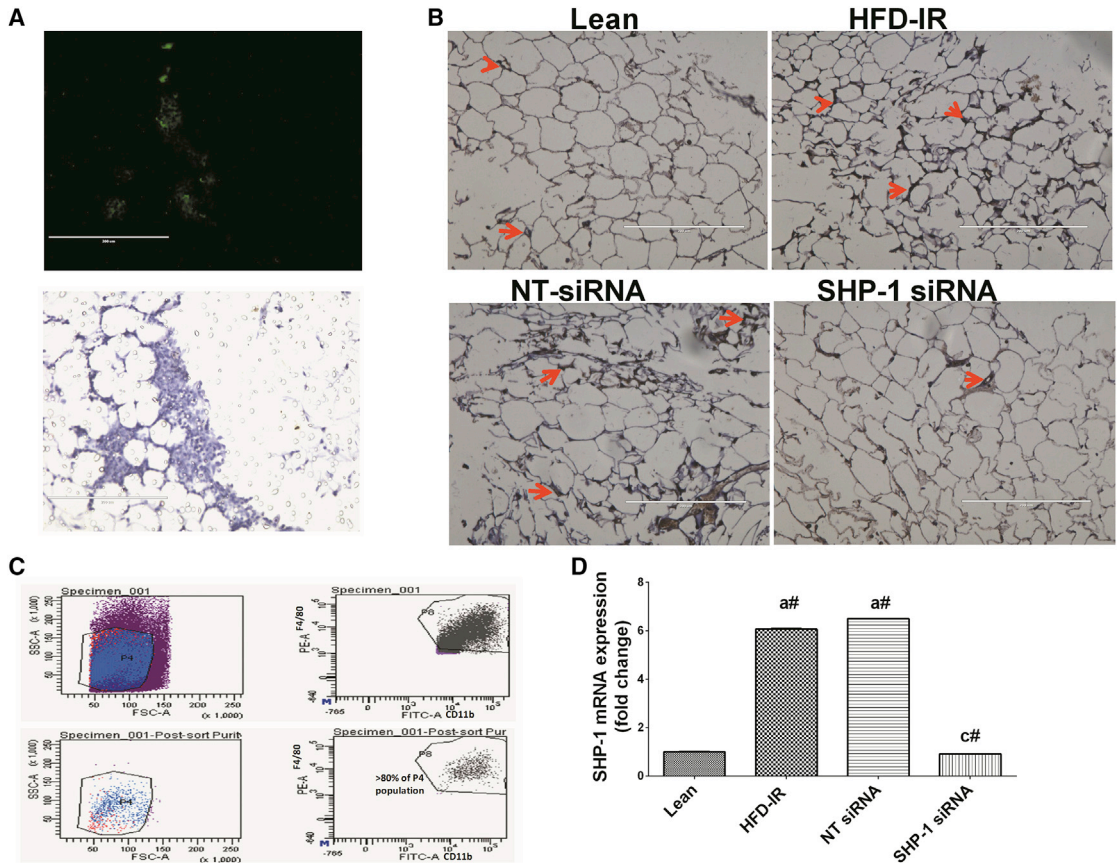

Figure 3. ATM Specific Deletion of SHP-1 in HFD-IR Mice

(A) Epididymal adipose tissue was isolated and stained with F4/80 antibody. Bright-field image of the stained area showing F4/80-positive cells (below) and fluorescence image showing localization of GPs near F4/80$^+$ cells (above) (scale bar, 200 μm). (B) Immunohistochemical analysis of adipose tissue stained with monoclonal anti-SHP-1 antibody. Grade 1, < 25% staining in lean mice; score 3, 50%–75% in HFD-IR mice and NT-siRNA mice; and grade 1, < 25% staining in SHP-1 siRNA group. Red arrows indicate staining areas. Scale bar, 200 μm. (C) Gating strategy to obtain adipose tissue macrophage populations. Based on forward scatter area (FSC-A) and side scatter area (SSC-A), cells were gated for size and granularity. F4/80$^+$ CD11b$^+$ high cells were then selected for sorting (upper), and the post-sorting purity of the cells was checked (lower). (D) SHP-1 mRNA expression measured by qPCR in adipose tissue macrophages isolated from epididymal adipose tissue. Results are means expressed in fold change (FC) ± SEM, n = 3. Statistical significance was determined by ANOVA Tukey post-test. $^{\#}p < 0.001$ when HFD-IR group and NT siRNA group was compared with lean group or SHP-1 siRNA group.

(402.8 ± 14.9 versus 302.2 ± 5.1 mg/dL), 30 (333 ± 6.9 versus 264 ± 7.4 mg/dL), and 60 min (266.6 ± 10.3 versus 173.8 ± 8.5 mg/dL) (Figure 4C). When compared to the HFD-IR group and NT siRNA group, the improved glucose homeostasis in the SHP-1 siRNA group was due to enhanced insulin sensitivity, which was observed as significantly decreased blood insulin levels at all time points (0, 15, 30, and 60 min) (Figures 4C and 4D). Comparing the NT siRNA group with the HFD-IR group, no significant difference was observed, which means NT siRNA does not affect glucose homeostasis. For all time points, the area under the curve was compared between the groups using a two-way ANOVA for diet and time interaction. The area under the curve for the OGTT and insulin test was significantly reduced in the SHP-1 siRNA group ($p < 0.001$) in comparison to the HFD-IR group and NT siRNA group, respectively (Figures 4E and 4F). Similarly, the homeostatic model assessment-insulin resistance (HOMA-IR) score for the SHP-1 siRNA group was found to be significantly lower in the SHP-1 siRNA group in comparison to the HFD-IR group and NT siRNA group (Figure 4G).

Further, we analyzed the effect of ATM SHP-1 silencing on lipid metabolism. The serum triglyceride levels in the SHP-1 siRNA group were not much changed in comparison to the HFD-IR group (165.0 ± 10.3 versus 179.9 ± 8.4 mg/dL) (Figure 1H). Similarly, serum cholesterol levels were also slightly decreased the SHP-1 siRNA group in comparison to the HFD-IR group (212.7 ± 10.2 versus 225.3 ± 16.1 mg/dL) (Figure 1I). The results obtained showed that ATM-specific SHP-1 deficiency ameliorates high-fat-diet-induced insulin resistance. However, it does not significantly improve conditions like obesity, hypertriglyceridemia, and hypercholesterolemia in C57BL/6JJ mice.

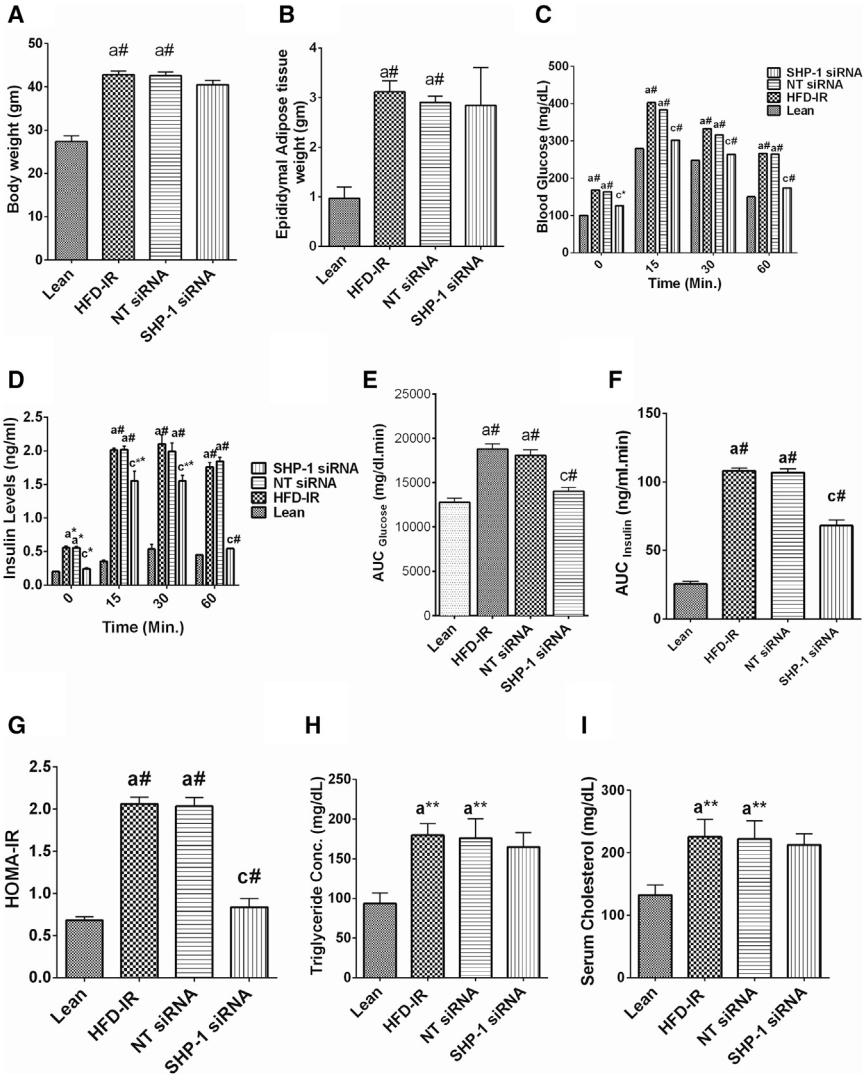

Figure 4. Metabolic Parameters

(A) Body-weight, (B) epididymal fat pads, (C) oral glucose tolerance test (OGTT), (D) insulin levels, (E) area under the curve (AUC) for OGTT graph, (F) AUC for insulin graph, (G) HOMA-IR, (H) serum triglyceride, and (I) serum cholesterol. 24 h after the last i.p injection, mice fasted for 12 h for the OGTT and insulin test. Statistically significant values are denoted by *$p < 0.05$, **$p < 0.01$, #$p < 0.001$ from one-way or two-way ANOVA when HFD-IR and NT-siRNA are compared with lean group and when SHP-1 siRNA group is compared with HFD-IR and NT-siRNA group. Values presented as mean ± SEM, n = 3–5.

Impact on AT Physiology

H&E staining of epididymal ATs suggested adipocyte hypertrophy in mice fed the HFD (Figure 5A). The number of cells per field was significantly reduced in HFD-IR mice, confirming an increased adipocyte size when compared to the lean group (Figure 5C). Interestingly, the size of the adipocyte from the SHP-1 siRNA group was slightly reduced in comparison to HFD-IR mice (Figure 5B). Also, the number of crown-like structures (CLSs), representing an accumulation of macrophages around adipocytes, was significantly decreased in the SHP-1 siRNA group in comparison to HFD-IR group (Figures 5D and 5E).

The flow cytometric analysis of the ATMs as F4/80 and CD11b double-positive cells showed a significant ~23% and ~37% increase in HFD-IR mice and NT siRNA mice, respectively, in comparison to the lean group (Figures 6A and 6B). Interestingly, the SHP-1 siRNA group showed a significant ($p < 0.01$) ~40% increase in F4/80 and CD11b double-positive cells when compared to the HFD-IR group (Figures 6A and 6B). Further, MCP-1 was also significantly elevated ($p < 0.01$) in HFD-IR mice (Figure 6C). The enhanced infiltration of macrophages into AT suggested by flow cytometric results was further confirmed by significantly ($p < 0.001$) increased levels of MCP-1 in the SHP-1 siRNA group (Figure 6C).

ATM-Specific Deletion of SHP-1 Improves Insulin Sensitivity via Downregulating F4/80$^+$ CD11b$^+$ CD11c$^+$ Cell Population

To test the hypothesis that SHP-1 deficiency ameliorates obesity-induced insulin resistance via modulating the macrophage phenotype, we isolated the SVF of epididymal AT from mice and performed flow cytometry to analyze the macrophage population. CD11b is an integrin present on leukocytes, F4/80 is an adhesion protein present on myeloid-derived macrophages, and CD11c is an integral membrane protein present on dendritic cells but also expressed by M1 macrophages. We observed that ATMs from HFD-IR mice showed a significantly ($p < 0.01$) higher percentage of F4/80$^+$ CD11b$^+$ CD11c$^+$ cells in comparison to lean mice (34.97% ± 2.4% versus 17.58% ± 0.52%), which demonstrates the skewing of the macrophage phenotype toward an M1 state in an obese condition[4] (Figures 7A and 7B). SHP-1 inhibition significantly reduced the F4/80$^+$ CD11b$^+$ CD11c$^+$ number in the SHP-1 siRNA group in comparison to the HFD-IR group and NT siRNA group (~27% and ~57%, respectively), suggesting that SHP-1 deficiency suppresses the M1 phenotype in obese AT (Figures 7A and 7B). On the other hand, F4/80$^+$ CD11b$^+$ CD11c$^-$ cells, which are considered M2 macrophages, were significantly ~21% and ~41% downregulated in the HFD-IR and NT siRNA group, respectively, when compared to the lean group (Figures 7A and 7C). ATM-specific SHP-1 silencing significantly increased ($p < 0.001$) the F4/80$^+$ CD11b$^+$ CD11c$^-$ cell population to 78.17%. This shows that SHP-1 downregulation in ATMs increases

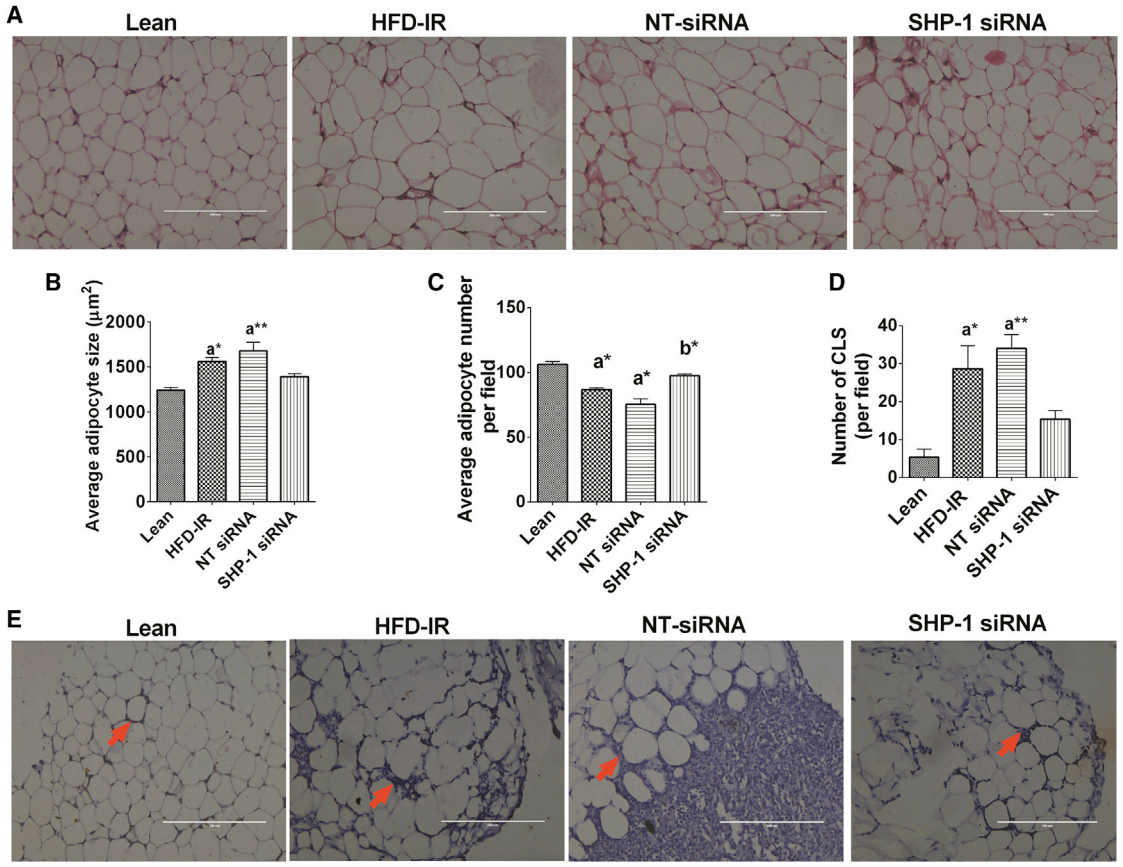

Figure 5. Adipose Tissue Physiology

(A) Representative photomicrographs of H&E-stained epididymal adipose tissue. (B) Adipocyte area. (C) Number of adipocytes per field. (D) Quantitative analysis of crown-like structure (CLS) formation. (E) Representative images of adipose tissue stained with anti-F4/80 antibody showing CLSs. Data are expressed as the mean ± SEM, n = 3–5 per group. Statistically significant values are denoted by *$p < 0.05$, **$p < 0.01$ from one-way ANOVA Tukey post-test when HFD-IR and NT-siRNA are compared with lean group and SHP-1 siRNA group is compared with HFD-IR and NT-siRNA group.

macrophage infiltration into AT but diminishes M1 state and increases M2 macrophages.

SHP-1 Deficiency Shifts ATMs toward an Anti-inflammatory Phenotype

ATMs were isolated and cultured for 24 hr to analyze the expression patterns for genes associated with classical (M1) and alternative (M2) activation viz. arginase 1 and inducible nitric oxide synthase (iNOS), and the levels of TNF-α, IL-6, and IL-10 were analyzed from supernatant collected after 24-hr incubation (Figures 7D–7H). Consistent with the previous reports, a trend toward the upregulation of some of the M1-associated genes and the downregulation of a subset of M2-associated genes in macrophages was observed in HFD-IR AT in comparison to the lean group. TNF-α, IL-6, and iNOS levels were upregulated almost 6-, 9-, and 1.6-fold, respectively, in ATMs from the HFD-IR group (Figure 7D–7F), whereas the expression of M2-associated IL-10 and arginase 1 was almost 3- and 2.5-fold downregulated, respectively (Figures 7G and 7H). There was no significant difference in the levels of all of the six inflammatory markers in the NT siRNA group in comparison to HFD-IR group. On the other hand, the SHP-1 siRNA group displayed upregulation of both M1-M2-specific markers. However, a significant increase was observed in M2-specific markers, whereas M1-specific markers showed the minor difference between the HFD-IR and siRNA group. There was a marginal increase in TNF-α, IL-6, and iNOS levels in the SHP-1 siRNA group in comparison to the HFD-IR group (Figures 7D–7F). On the other hand, M2-associated markers viz. IL-10 and arginase 1 were also significantly 2.2-fold and 2-fold upregulated in the SHP-1 siRNA group when compared to the HFD-IR group (Figures 7G and 7H).

This shows that SHP-1 deficiency increases macrophage infiltration but balances inflammatory nature of ATMs via modulating both M1-M2 characters leading to improved glucose homeostasis.

DISCUSSION

Genetic manipulation of ATM-specific genes has emerged as a promising strategy to treat obesity-associated insulin resistance. In

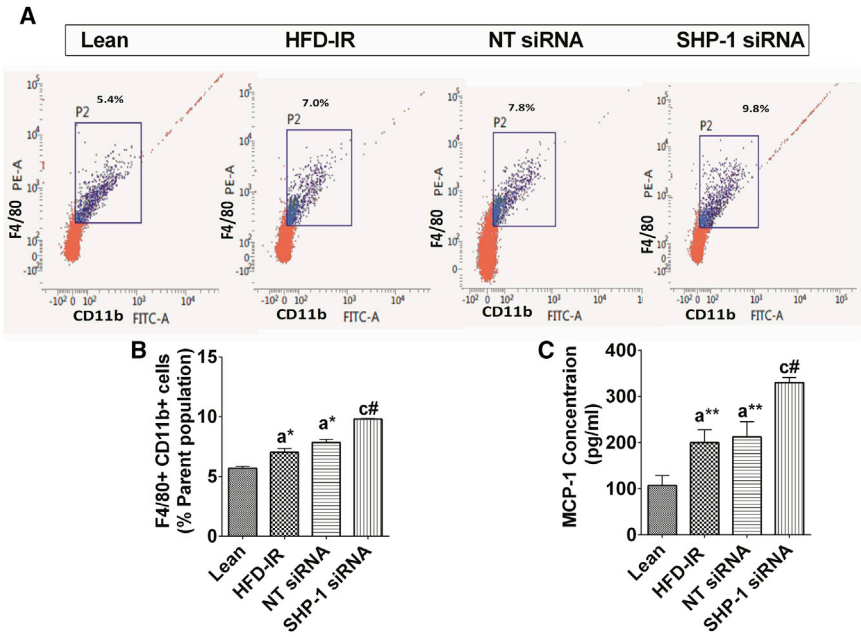

Figure 6. Effect on Adipose Tissue Macrophage Infiltration

(A and B) Plots (A) and graph (B) showing flow cytometric analysis of the stromal vascular fraction of epididymal adipose tissue stained with macrophage surface markers F4/80 (PE-conjugated monoclonal antibody) and CD11b (FITC-conjugated monoclonal antibody). (C) MCP-1 levels analyzed by ELISA. Data are expressed as the mean ± SEM, n = 3 per group. Statistically significant values are denoted by *p < 0.05, **p < 0.01, #p < 0.001 from one-way ANOVA Tukey post-test when HFD-IR and NT-siRNA are compared with the lean group and when SHP-1 siRNA group is compared with HFD-IR and NT-siRNA group.

the present work, using GP, we investigated the role of SHP-1, a protein tyrosine phosphatase, in improving glucose homeostasis via modulating AT inflammation and the macrophage phenotype during diet induced-obesity. We observed that SHP-1 inhibition resulted in improved glucose tolerance and insulin sensitivity. This is because SHP-1 inhibition was associated with the reduction in pro-inflammatory macrophage population (M1), increased M2 macrophage population, reduced CLSs, adipocyte hypertrophy, and modulation of inflammatory molecules in AT. Therefore, our study explored an unknown functional role of SHP-1 in modulating the macrophage phenotype and inflammation in obese AT.

Using a diet-induced obesity model with ATM-specific SHP-1 silencing, our current study revealed that SHP-1 inhibition had no effect on the development of obesity and did not significantly affect body weight or fat pad weight. Earlier, several reports showed improved insulin sensitivity and reduced AT inflammation independent of weight loss in obese mice.[8] Furthermore, SHP-1 silencing significantly improved glucose tolerance and insulin sensitivity. Although the link between SHP-1 deficiency and enhanced insulin signaling has been reported in obese mouse models with genetic or pharmacological inhibition of ubiquitously expressed SHP-1, ATM-specific SHP-1 inhibition had not been performed earlier. This is important because the improvement in metabolic character via site-specific gene silencing is more beneficial as a therapeutic strategy rather than whole-body gene silencing, which may affect functions of a target gene in other tissues. For example, ubiquitous deletion of SHP-1 in motheaten or viable motheaten mice improves glucose tolerance, but it also induces autoimmunity and immunodeficiency leading to a shorter lifespan.

AT expansion during chronic overnutrition increases macrophage accumulation and activation leading to insulin resistance. Therefore, we investigated whether improved insulin sensitivity in SHP-1-deficient mice is attributed to AT remodeling or not. Histological analysis of AT from HFD-IR mice showed adipocyte hypertrophy indicated by significantly increased adipose size and decreased cell number in comparison to lean mice, which were modestly altered in the SHP-1 siRNA group. This indicates that obesity-associated enhanced SHP-1 expression limits AT expansion to inhibit release of pro-inflammatory mediators that can engender insulin resistance. Lodeiro et al.[19] demonstrated the role of SHP-1 as a negative regulator of ghrelin (hunger hormone) signaling and showed the varying response of SHP-1 to chronic overnutrition in different adipose depots. We concluded that it might be possible that since SHP-1 is a negative regulator of insulin signaling, SHP-1 deficiency augments insulin signaling in the initial phase and helps in AT remodeling at the later phase, as signified by a modest reduction in adipocyte size. However, further studies are required to establish the role of SHP-1 in regulating AT remodeling during obesity.

ATMs surround moribund adipocytes forming a structure called "CLSs," a hallmark of obese AT. The localization of SHP-1 in CLSs indicates that SHP-1 is predominantly expressed by adipose-tissue-resident macrophages. We observed that deletion of ATM-specific SHP-1 limits the number of CLSs in the AT in comparison to HFD-IR group. Reportedly, SHP-1 induces apoptosis via inhibiting STAT-3, and SHP-1 deficiency could lead to STAT-3 activation, thus rescuing the adipocyte from apoptosis. We hypothesize that SHP-1 deficiency might suppress adipocyte apoptosis, thus decreasing CLS number.

A point to ponder is how SHP-1 deficiency improves insulin sensitivity while increasing macrophage infiltration into the AT as observed by flow cytometric analysis of $F4/80^+$ $CD11b^+$ double-positive cells and MCP-1 levels. Therefore, next, we checked the phenotype-specific markers of ATMs. $F4/80^+$ $CD11b^+$ $CD11c^+$ cells, which

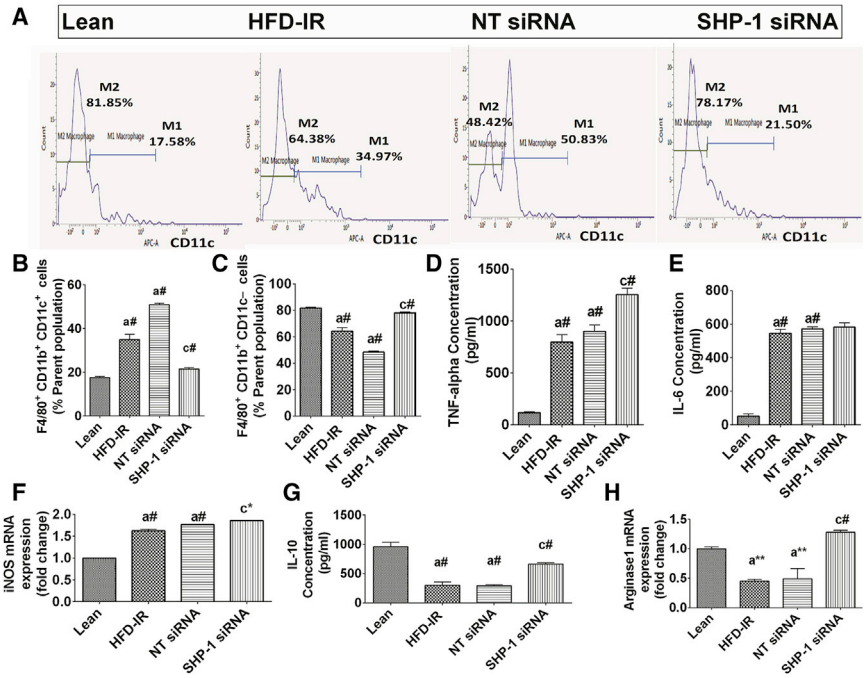

Figure 7. Effect of ATM-Specific SHP-1 Deletion on the Macrophage Phenotype

(A) Flow cytometric analysis of the stromal vascular fraction of epididymal adipose tissue stained with macrophage surface markers F4/80 (PE-conjugated monoclonal antibody), CD11b (FITC-conjugated monoclonal antibody), and CD11c (APC-conjugated monoclonal antibody). Samples were gated for (B) F4/80$^+$ CD11b$^+$ CD11c$^+$ cells and (C) F4/80$^+$ CD11b$^+$ CD11c$^-$ cells. The cytokine levels of (D) TNF-α, (E) IL-6, and (G) IL-10 were measured by ELISA. Relative mRNA expression of (F) iNOS and (H) arginase 1 was analyzed by qPCR. Data are expressed as the mean ± SEM, n = 3 per group. Statistically significant values are denoted by *p < 0.05, **p < 0.01, #p < 0.001 from one-way ANOVA Tukey post-test when HFD-IR and NT-siRNA are compared with lean group and when SHP-1 siRNA group is compared with HFD-IR and NT-siRNA group.

are considered as M1 macrophages, were significantly reduced in the SHP-1 siRNA group in comparison to the HFD-IR group. This finding suggested that though SHP-1 deficiency increases macrophage infiltration, it suppresses their classical activation. Contrastingly, M2 macrophage population (F4/80$^+$ CD11b$^+$ CD11c$^-$) showed an upsurge in the SHP-1 siRNA group, thereby giving a clue that SHP-1 possibly promotes M1 cells while limiting the M2 phenotype. Recently, the role of SHP-1 in promoting M1 differentiation of macrophages in virus-induced myositis and limiting alternative activation of macrophages by inhibiting IL-4/STAT-6 axis in obesity model has been reported.[15,20]

Being a multifunctional molecule, SHP-1's functions vary with disease and tissue type. Therefore, to further delineate the macrophage phenotype, we analyzed a subset of macrophage-phenotype-specific markers, namely arginase 1, iNOS, IL-6, IL-10, and TNF-α. Interestingly, in the SHP-1 siRNA group there was an upregulation in the levels of all the markers; however, M1-specific markers (iNOS, IL-6, and TNF-α) were modestly upregulated, whereas there was a significant increase in M2 markers (arginase 1 and IL-10). The upregulation of pro-inflammatory genes including TNF-α and IL-6 has been exhibited by SHP-1-deficient macrophages in neuronal diseases.[20] Also, high levels of arginase 1 have been observed in CNS glia of SHP-1-deficient mice.[21] It is conceived that SHP-1 regulates the balance between the arginase 1 and iNOS signaling pathways. Nevertheless, these studies were performed using mouse models with systemic SHP-1 deficiency.

We conclude that ATM-specific SHP-1 deficiency creates a homeostatic milieu in AT via balancing M1 and M2 status and thereby regulates AT inflammation, leading to improved glucose homeostasis. Therefore, targeting ATM-specific SHP-1 using glucan-particle-encapsulated antagonists could be of immense therapeutic use for the treatment of obesity-associated insulin resistance.

CONCLUSION

In the present study, glucan-particle-based targeted SHP-1 silencing in ATMs unveiled the function of SHP-1 as a regulator of macrophage polarization associated with the pathogenesis of obesity-related insulin resistance. Therefore, SHP-1 could be a potential therapeutic target for the treatment of obesity-related insulin resistance and other disorders involving macrophage polarization. Further, identification of SHP-1 antagonist and their encapsulation into the GP could be the addition to the targeted drug delivery system for the treatment of obesity-related insulin resistance.

MATERIALS AND METHODS

Materials

ON-TARGETplus Ptpn6 (SHP-1) siRNA and nontargeting siRNA were obtained from Dharmacon, USA. FITC was purchased from Invitrogen, USA. Cy7 NHS ester was purchased from Click Chemistry Tools (AZ, USA). EP was obtained from Gene Tools, USA. All the cell culture reagents were purchased from Gibco, USA. RAW264.7 cell line was procured from National Centre for Cell Science (NCCS), Pune, India. Mouse insulin assay kit was purchased from Mercer EXPert Assays, USA. Allophycocyanin (APC) anti-mouse CD11c antibody, PE anti-mouse F4/80 antibody, FITC anti-mouse CD11b antibody, and stain buffer were from BD Biosciences, USA. TNF-α ELISA kit, IL-6 ELISA kit, IL-10 ELISA kit, IFN-γ ELISA kit, and MCP-1 ELISA kit were obtained from Krishgen Biosystems, USA. Anti-mouse SHP-1 antibody was from Abcam, UK, and anti-mouse F4/80 was from R&D Systems, USA. The 40-μm cell strainer was

purchased from Corning, USA, and 100-μm membrane filters were from EMD Millipore, USA. RNA isolation kit (FASTRNA Pro Green Kit) was from MP Biomedicals, USA. DAPI and single-step qPCR kit were from Sigma, USA. All other reagents were obtained from Sigma-Aldrich (MO, USA).

Preparation of GPs

GPs were prepared as described previously.[22] In brief, *Saccharomyces cerevisiae* (50 g of SAF-Mannan) was suspended in 0.5 L of 0.5 M NaOH and heated to 80°C for 1 h. The suspension was spun at 200 × *g* for 10 min, and the insoluble material containing the yeast cell walls was collected and re-suspended in 0.5 L of 0.5 M NaOH and again heated to 80°C for 1 h. The insoluble material was collected by centrifugation and washed three times each with 1 L of water, 200 mL of isopropanol, and 200 mL of acetone. The resulting slurry was dried at room temperature to produce GPs powder.

Fluorescent Labeling of GPs

GPs (1 g) were washed with 0.1 M sodium carbonate buffer (pH 9.2) and resuspended in 0.1 L carbonate buffer. To label the GPs, 5-(4,6-dichlorotriazinyl) aminofluorescein (FITC) or Cy7 NHS ester was added to the buffered glucan shell suspension and incubated at room temperature in the dark overnight. Then, 2 mM Tris buffer was added and incubated for 15 min. GPs were then repeatedly washed with sterile water until the unbound dye is removed. Finally, the FITC-tagged or Cy7-tagged GPs were flash-frozen and lyophilized in the dark.

Preparation and Characterization of the EP-siRNA Complex and siRNA-Loaded GPs

The siRNA-EP complex was formed by incubating 3 nmol siRNA with 50 nmol EP in sodium acetate buffer (30 mM, pH 4.8) at room temperature for 15 min in a final volume of 20 μL. The siRNA-EP solution was then added to GPs (~1 mg), vortexed, and incubated for 1 h. Finally, the siRNA-loaded GPs were resuspended in PBS, sonicated, and stored at 4°C for further use. The average particle size and zeta potential measurements were done by Zetasizer-nano analyzer Zs (Malvern Instruments, Worcestershire, UK). Mean values were obtained from three runs at 25°C.

Cell Culture

RAW264.7, a murine monocyte cell line, was procured from NCCS, Pune, India. Cells were cultured in DMEM containing 10% fetal bovine serum (FBS) and antibiotic-antimycotic solution (100 IU/mL). About 150 pmol SHP-1 siRNA complexed with 3 nmol EP was added to cells cultured per well of a 12-well plate, and afterward, 48 h cells were harvested for further analysis. To analyze the cellular uptake of GPs, FITC-labeled GPs were added to the cultured RAW264.7 cells and counterstained with DAPI nuclear stain for confocal imaging.

GPs Administration and AT Isolation

Male C57BL/6J mice were randomly divided into four groups: the control group (lean mice, n = 15) received a standard rodent diet, the HFD-IR group (HFD-IR mice, n = 15) received a HFD (60% fat, 20% carbohydrate, and 20% protein), the control siRNA group (NT siRNA, n = 15) was injected with GPs containing nontargeting control siRNA in addition to HFD, and the SHP-1 siRNA group (SHP-1 siRNA, n = 15) was injected with GPs containing SHP-1 siRNA in addition to HFD. The HFD was prepared as described previously.[23] The dietary regimen lasted for 16 weeks, and 0.2 mg GPs containing 0.6 nmol siRNA and 10 nmol EP were intra-peritoneally injected every alternate day for a period of 2 weeks. At the end of the study, animals were sacrificed and epididymal AT was collected for further studies. The animal study was approved and performed in accordance with the guidelines of the University's Animal Ethics Committee (173/GO/Re/S/2000/CPCSEA).

Metabolic Studies

Twenty-four hours after the last i.p. injection, the mice were fasted overnight and subjected to an OGTT. For OGTT, a basal blood sample was collected from the tail vein at 0 min, and blood glucose levels were measured. Then, the mice were gavaged with 1.5 g glucose/kg of body weight and blood glucose levels were further monitored at 15, 30, and 60 min using glucose oxidase method. Blood insulin levels were also measured at 0, 15, 30, and 60 min using a mouse insulin ELISA kit. The area under the curve (AUC) for blood glucose was calculated using a two-way ANOVA for diet and time interaction.[24] The HOMA-IR score was calculated as described previously.[25] Serum triglyceride and cholesterol levels were estimated using commercial kits from BioAssay Systems, USA.

In Vivo Imaging

The high-fat-diet-fed mice were injected with Cy7-labeled GPs, and the *in vivo* imaging of the localized GPs was performed. Fluorescence signals were acquired with a 753-nm and 800-nm excitation and emission filter, respectively, using the IVIS spectrum imaging system (PerkinElmer, USA). Results are presented on a color scale overlaid on a grayscale photograph of the mice, and the signals were quantified as total radiant efficiency ([photons/s]/[μW/cm^2]) using Living Image software. Four hours post-injection, mice were euthanized and tissues were dissected for *ex vivo* imaging.

Immunohistochemistry and Microscopy

Paraffin-embedded AT sections (6 μm) were immunostained with monoclonal anti-SHP-1 (ab32559, 1:100) and anti-F4/80 antibody (MAB5580, 10 μg/mL) for immunohistochemical analysis. The bright-field and fluorescence images (GFP filter) of the stained sections were captured by EVOS FLc imaging system (Thermo Fisher Scientific, USA).

Adipocyte Size Measurement

Epididymal AT was fixed, and paraffin-embedded sections (6 μm) were cut and stained with H&E stains. Pictures were taken in the bright field, and adipocyte size was measured with adiposoft software automatically (Adiposoft).[26] The program errors such as missing adipocytes or clustering of two adipocytes were corrected manually.

Immunophenotyping and FACS

The SVF containing macrophages was isolated from the epididymal fat pad of mice as described earlier using collagenase II method.[23] In brief, epididymal AT was isolated, finely chopped, and incubated with collagenase II, and the cell suspension obtained was filtered through a 100-μm membrane filter and centrifuged. The SVF pellet obtained containing macrophages was stained with the macrophage surface markers (F4/80-PE, CD11b-FITC, CD11c-APC). For immunophenotyping, the cells were washed with stain buffer (BD Biosciences, USA) and spun for 5 min at 300 × *g* at 4°C. 10^6 cells/mL were incubated with fluorescent antibodies (BD Biosciences) for 30 min in dark at 4°C. Cells were rewashed to remove the unbound antibodies. The cell pellet obtained was re-suspended in 0.5 mL stain buffer and analyzed using BD FACSVerse (BD Biosciences). Unstained and single-stained samples were used for compensation to avoid spectral overlap. For ATM sorting, SVF was stained with F4/80-PE and CD11b-FITC, filtered through a 40-μm cell strainer, and separated using a BD FACSAria III cell sorter (BD Biosciences, California, USA). The purity of the fluorescence-activated cell sorting (FACS)-sorted fraction was determined by post-sort analysis.

ELISA

ATMs were cultured for 24 h in DMEM with 10% FBS, and thereafter, the supernatant was collected to measure the levels of IL-6, IL-10, TNF-α, and MCP-1 using their respective kits according to the manufacturer's instruction (Krishgen Biosystems, USA).

qPCR

ATMs were sorted (purity > 80%), and total RNA was isolated from ATMs using FASTRNA pro green kit (MP Biochemicals), and 100 ng of total RNA was reverse transcribed and amplified using the single-step qPCR kit (Sigma, USA) on Roche LC 480 light cycler (Roche, USA). The relative quantification of the mRNA levels were measured by using the following primer pairs: SHP-1 forward, 5′-AGAGA CGTTTGACAGCCTCA-3′; SHP-1 reverse, 5′-TCCGACTCCTGCT TCTTGTT-3′; iNOS forward, 5′-CAGAGGACCCAGAGACAA GC-3′; iNOS reverse, 5′-TGCTGAAACATTTCCTGTGC-3′; Arg1 forward, 5′-AAGAAAAGGCCGATTCACCT-3′; Arg1 reverse, 5′-CACCTCCTCTGCTGTCTTCC-3′; β-actin forward, 5′-TACAGC TTCACCACCACAGC-3′; β-actin reverse, 5′-AAGGAAGGCTGG AAAAGAGC-3′; and fold change was normalized to β-actin expression and assessed using the $2^{-\Delta\Delta ct}$ calculation method.[27]

Statistical Analysis

Data were statistically analyzed using GraphPad Prism software (version 6.0). All values are presented as mean ± SEM. The comparison between two groups was done using unpaired t test and between three groups using one-way ANOVA Tukey post-test. For OGTT and insulin test, the statistical significance was measured using two-way ANOVA Tukey post-test. The p values < 0.05 were considered statistically significant.

SUPPLEMENTAL INFORMATION

Supplemental Information can be found online at https://doi.org/10.1016/j.omtn.2019.04.020.

AUTHOR CONTRIBUTIONS

F.K., Y.S., A.A. were involved in project planning, data analysis, and manuscript preparation. A.B. was involved in project planning. Y.S., P.S.Y., and S.K.M. performed experimental work.

CONFLICTS OF INTEREST

The authors declare no conflict of interest.

ACKNOWLEDGMENTS

We appreciate research funding by the Department of Health Research (DHR), Ministry of Health and Family Welfare, and the government of India (DHR/HRD fellow/start up project/4/2013-14). Y.S. is highly thankful to the University Grants Commission for providing SRF (2061030742) and the Council of Scientific and Industrial Research, India for providing a Research Associateship (312362/2K17/1). We are highly thankful to Dr. Pradeep Rai (application scientist) and Dr. Vinay Gupta (senior application scientist), BD-JHFACS Academy, Jamia Hamdard, New Delhi, India, for their help in the flow cytometry experiment and data analysis. The authors wish to thank Mr. Amit Kumar, application specialist (Malvern Panalytical) for DLS analysis. Histological and immunohistochemical analysis of AT by Dr. Ambrish Tiwari (Veterinary Pathologist) is highly acknowledged.

REFERENCES

1. Fischer, I.P., Irmler, M., Meyer, C.W., Sachs, S.J., Neff, F., Hrabě de Angelis, M., Beckers, J., Tschöp, M.H., Hofmann, S.M., and Ussar, S. (2018). A history of obesity leaves an inflammatory fingerprint in liver and adipose tissue. Int. J. Obes. *42*, 507–517.

2. Kralova Lesna, I., Kralova, A., Cejkova, S., Fronek, J., Petras, M., Sekerkova, A., Thieme, F., Janousek, L., and Poledne, R. (2016). Characterisation and comparison of adipose tissue macrophages from human subcutaneous, visceral and perivascular adipose tissue. J. Transl. Med. *14*, 208.

3. Oh, D.Y., Morinaga, H., Talukdar, S., Bae, E.J., and Olefsky, J.M. (2012). Increased macrophage migration into adipose tissue in obese mice. Diabetes *61*, 346–354.

4. Lumeng, C.N., Bodzin, J.L., and Saltiel, A.R. (2007). Obesity induces a phenotypic switch in adipose tissue macrophage polarization. J. Clin. Invest. *117*, 175–184.

5. Lumeng, C.N., and Saltiel, A.R. (2011). Inflammatory links between obesity and metabolic disease. J. Clin. Invest. *121*, 2111–2117.

6. Odegaard, J.I., Ricardo-Gonzalez, R.R., Goforth, M.H., Morel, C.R., Subramanian, V., Mukundan, L., Red Eagle, A., Vats, D., Brombacher, F., Ferrante, A.W., and Chawla, A. (2007). Macrophage-specific PPARgamma controls alternative activation and improves insulin resistance. Nature *447*, 1116–1120.

7. Aouadi, M., Tencerova, M., Vangala, P., Yawe, J.C., Nicoloro, S.M., Amano, S.U., Cohen, J.L., and Czech, M.P. (2013). Gene silencing in adipose tissue macrophages regulates whole-body metabolism in obese mice. Proc. Natl. Acad. Sci. USA *110*, 8278–8283.

8. Lee, J.T., Pamir, N., Liu, N.C., Kirk, E.A., Averill, M.M., Becker, L., Larson, I., Hagman, D.K., Foster-Schubert, K.E., van Yserloo, B., et al. (2014). Macrophage metalloelastase (MMP12) regulates adipose tissue expansion, insulin sensitivity, and expression of inducible nitric oxide synthase. Endocrinology *155*, 3409–3420.

9. Kim, J., Chung, K., Choi, C., Beloor, J., Ullah, I., Kim, N., Lee, K.Y., Lee, S.K., and Kumar, P. (2016). Silencing CCR2 in macrophages alleviates adipose tissue

inflammation and the associated metabolic syndrome in dietary obese mice. Mol. Ther. Nucleic Acids *5*, e280.

10. Dubois, M.J., Bergeron, S., Kim, H.J., Dombrowski, L., Perreault, M., Fournès, B., Faure, R., Olivier, M., Beauchemin, N., Shulman, G.I., et al. (2006). The SHP-1 protein tyrosine phosphatase negatively modulates glucose homeostasis. Nat. Med. *12*, 549–556.

11. Xu, E., Charbonneau, A., Rolland, Y., Bellmann, K., Pao, L., Siminovitch, K.A., Neel, B.G., Beauchemin, N., and Marette, A. (2012). Hepatocyte-specific Ptpn6 deletion protects from obesity-linked hepatic insulin resistance. Diabetes *61*, 1949–1958.

12. Krüger, J., Wellnhofer, E., Meyborg, H., Stawowy, P., Östman, A., Kintscher, U., and Kappert, K. (2016). Inhibition of Src homology 2 domain-containing phosphatase 1 increases insulin sensitivity in high-fat diet-induced insulin-resistant mice. FEBS Open Bio *6*, 179–189.

13. Sharma, Y., Bashir, S., Ansarullah, Faraz Khan, M., Ahmad, A., and Khan, F. (2017). Inhibition of Src homology 2 domain containing protein tyrosine phosphatase as the possible mechanism of metformin-assisted amelioration of obesity induced insulin resistance in high fat diet fed C57BL/6J mice. Biochem. Biophys. Res. Commun. *487*, 54–61.

14. Christophi, G.P., Panos, M., Hudson, C.A., Christophi, R.L., Gruber, R.C., Mersich, A.T., Blystone, S.D., Jubelt, B., and Massa, P.T. (2009). Macrophages of multiple sclerosis patients display deficient SHP-1 expression and enhanced inflammatory phenotype. Lab. Invest. *89*, 742–759.

15. Zheng, C., Yang, Q., Xu, C., Shou, P., Cao, J., Jiang, M., Chen, Q., Cao, G., Han, Y., Li, F., et al. (2015). CD11b regulates obesity-induced insulin resistance via limiting alternative activation and proliferation of adipose tissue macrophages. Proc. Natl. Acad. Sci. USA *112*, E7239–E7248.

16. Soto, E.R., O'Connell, O., Dikengil, F., Peters, P.J., Clapham, P.R., and Ostroff, G.R. (2016). Targeted delivery of glucan particle encapsulated gallium nanoparticles inhibits HIV growth in human macrophages. J. Drug Deliv. *2016*, 8520629.

17. Chen, H., Dorrigan, A., Saad, S., Hare, D.J., Cortie, M.B., and Valenzuela, S.M. (2013). In vivo study of spherical gold nanoparticles: inflammatory effects and distribution in mice. PLoS ONE *8*, e58208.

18. Bu, L., Gao, M., Qu, S., and Liu, D. (2013). Intraperitoneal injection of clodronate liposomes eliminates visceral adipose macrophages and blocks high-fat diet-induced weight gain and development of insulin resistance. AAPS J. *15*, 1001–1011.

19. Lodeiro, M., Alén, B.O., Mosteiro, C.S., Beiroa, D., Nogueiras, R., Theodoropoulou, M., Pardo, M., Gallego, R., Pazos, Y., Casanueva, F.F., and Camiña, J.P. (2011). The SHP-1 protein tyrosine phosphatase negatively modulates Akt signaling in the ghrelin/GHSR1a system. Mol. Biol. Cell *22*, 4182–4191.

20. Watson, N.B., Schneider, K.M., and Massa, P.T. (2015). SHP-1-dependent macrophage differentiation exacerbates virus-induced myositis. J. Immunol. *194*, 2796–2809.

21. Christophi, G.P., Hudson, C.A., Gruber, R.C., Christophi, C.P., Mihai, C., Mejico, L.J., Jubelt, B., and Massa, P.T. (2008). SHP-1 deficiency and increased inflammatory gene expression in PBMCs of multiple sclerosis patients. Lab. Invest. *88*, 243–255.

22. Soto, E.R., and Ostroff, G.R. (2008). Characterization of multilayered nanoparticles encapsulated in yeast cell wall particles for DNA delivery. Bioconjug. Chem. *19*, 840–848.

23. Bashir, S., Sharma, Y., Elahi, A., and Khan, F. (2016). Amelioration of obesity-associated inflammation and insulin resistance in c57bl/6 mice via macrophage polarization by fish oil supplementation. J. Nutr. Biochem. *33*, 82–90.

24. Williams, L.M., Campbell, F.M., Drew, J.E., Koch, C., Hoggard, N., Rees, W.D., Kamolrat, T., Thi Ngo, H., Steffensen, I.L., Gray, S.R., and Tups, A. (2014). The development of diet-induced obesity and glucose intolerance in C57BL/6 mice on a high-fat diet consists of distinct phases. PLoS ONE *9*, e106159.

25. van der Heijden, R.A., Sheedfar, F., Morrison, M.C., Hommelberg, P.P., Kor, D., Kloosterhuis, N.J., Gruben, N., Youssef, S.A., de Bruin, A., Hofker, M.H., et al. (2015). High-fat diet induced obesity primes inflammation in adipose tissue prior to liver in C57BL/6j mice. Aging (Albany N.Y.) *7*, 256–268.

26. Castrillon, J., Huston, W., and Bengtson Nash, S. (2017). The blubber adipocyte index: A nondestructive biomarker of adiposity in humpback whales (*Megaptera novaeangliae*). Ecol. Evol. *7*, 5131–5139.

27. Livak, K.J., and Schmittgen, T.D. (2001). Analysis of relative gene expression data using real-time quantitative PCR and the 2(-Delta Delta C(T)) Method. Methods *25*, 402–408.